nature communications

Article

https://doi.org/10.1038/s41467-026-70876-4

Reactivating exhausted tumor-infiltrating T cells by a bispecific DC-T cell engager in mice

Received: 13 May 2025

Accepted: 3 March 2026

Published online: 17 March 2026

Check for updates

Xuhao Zhang[1,2,3,4,12] ✉, Yu Gao[2,3,4,12], Wenbo Hu[2,4,12], Yong Liang[2,4], Xiaozhe Yin[2,3,4], Xiangjun Shi[2,5], Hongjia Li[6,7], Huiping Liao[8], Jingya Guo[6,7], Xiaohong Yu[8], Mingzhao Zhu[9], Hua Peng[10,11], Wenyan Wang[2,4] ✉ & Yang-Xin Fu[2,4,8] ✉

Tumor infiltrating T cells (TIL) are key players in the anti-tumor immune response. However, chronic exposure to tumor-derived antigens drives the differentiation into 'exhausted' TILs. Whether intratumoral dendritic cells (DC) can mitigate TILs exhaustion and maintain function is unclear. Here, we develop a bispecific DC-T cell engager (BiDT), consisting of an anti-TIM3-IFN fusion protein, and demonstrate that, in preclinical mouse tumor models, this engager simultaneously targets TIM3 on exhausted TILs and activates DCs via the IFNAR receptor. Mechanistically, BiDT reactivates exhausted TIM3^{+}TILs by preventing apoptosis through increased Bcl-2 expression and enhances DC function to reactivate T cells via IL-2 signalling and co-stimulatory CD80/86-CD28 interactions within the tumor microenvironment. Finally, to mitigate IFNα-induced toxicity, we engineer a Pro-BiDT engager featuring a pro-IFNα and report potent antitumor activity with reduced systemic toxicity. Thus, by bridging DC-T cells together, BiDT treatment enhances the critical communication pathways and cellular circuits necessary for effective anti-tumor immunity.

Tumor-infiltrating lymphocytes (TIL), especially tumor-specific T cells, are essential components of antitumor immunity and serve as critical targets for cancer immune defense[1]. Within the tumor microenvironment (TME), chronic antigen exposure drives tumor-specific TILs to differentiate into the exhausted state[2,3]. Exhausted T cells are marked by upregulation of immune checkpoints molecules, diminished capacity for cytokine production and proliferation, and in some cases, apoptotic cell death. This dysfunctional state is frequently associated with ineffective tumor control[4]. Consequently, revitalizing exhausted T cells is a promising strategy for restoring antitumor immunity. T cell immunoglobulin and mucin domain-containing protein 3 (TIM3) is an immune checkpoint molecule that is essential for optimal effector T cell responses and contributes to T cell exhaustion[5]. Although in vivo blockade of TIM3 signaling can partially alleviate T cell exhaustion, its limited efficacy underscores that monotherapy targeting a single immune checkpoint often yields suboptimal outcomes[6]. Therefore, strategies to effectively reverse T cell exhaustion need further investigation.

[1]Institute for Data-Driven Tumor Immunology, Chongqing Medical University, Chongqing, China. [2]School of Basic Medical Sciences, Tsinghua University, Beijing, China. [3]Tsinghua-Peking Center for Life Sciences, Tsinghua University, Beijing, China. [4]State Key Laboratory of Molecular oncology, Tsinghua University, Beijing, China. [5]China National Clinical Research Center for Neurological Diseases, Beijing Tiantan Hospital, Capital Medical University, Beijing, China. [6]National Laboratory of Biomacromolecules, Institute of Biophysics, Chinese Academy of Sciences, Beijing, China. [7]University of Chinese Academy of Sciences, Beijing, China. [8]Changping Laboratory, Beijing, China. [9]CAS Key Laboratory of Pathogen Microbiology and Immunology, Institute of Microbiology, Chinese Academy of Sciences, Beijing, China. [10]Guangzhou National Laboratory, Bio-Island, Guangzhou, China. [11]State Key Laboratory of Respiratory Disease, National Clinical Research Center for Respiratory Disease, Guangzhou Institute of Respiratory Health, The First Affiliated Hospital of Guangzhou Medical University, Guangzhou, China. [12]These authors contributed equally: Xuhao Zhang, Yu Gao, Wenbo Hu.
✉e-mail: xuhaozhang@cqmu.edu.cn; wywang2022@tsinghua.edu.cn; yangxinfu@tsinghua.edu.cn

Dendritic cell (DC) in tumor-draining lymph nodes (TDLN) is critical for initiating naive T-cell priming[7]. During this process, CD28 engagement on T cells by CD80/86 expressed on DCs amplifies T-cell receptor (TCR) signaling by up to 100-fold[8–10]. Importantly, this co-stimulation increases IL-2 production and enhances the intrinsic capacity of T cells to resist apoptosis[11]. In contrast to the well-established role in TDLNs, the function of DCs within the TME in relation to T cell exhaustion or reactivation remains poorly defined. We hypothesize that productive crosstalk between intratumoral DCs and exhausted T cells could mitigate exhaustion or even re-activate T cells. However, such functional crosstalk requires fully activated DCs within the TME. Various immunosuppressive factors within the TME impair DC function by inhibiting their maturation and antigen presentation while upregulating checkpoint protein expression, thereby disrupting the DC-T cell interactions[12,13]. Type I interferons (IFN-I) are potent cytokines capable of rejuvenating intratumoral DCs, enhancing their antigen processing and presentation capacity to promote more effective T cell priming and re-activation[14,15]. Nevertheless, IFN-I expression in the TME is often limited or suppressed due to multiple mechanisms, including increased degradation of tumor-derived DNA and antigens, as well as defective cGAS-STING pathway signaling in certain tumor cells[16,17]. The clinical utilization of IFN-I is also limited due to severe systemic toxicity when delivered systemically[18].

Here, we develop a bispecific DC-T cell engager (BiDT) based on an anti-TIM3-IFNα fusion protein that enhances DC-T cell crosstalk in the TME. This molecule simultaneously activates DC and reactivates exhausted TILs. A tumor-activated prodrug variant (Pro-BiDT) retains potent anti-tumor activity while reducing systemic toxicity. This approach provides a strategy to locally reprogram immunosuppressive niches and may help overcome resistance to current immunotherapies.

Results

Tumor-reactive T cells are exhausted inside advanced tumors

Tumor-reactive T cells within the TME frequently undergo exhaustion following prolonged exposure to tumor antigens, a state marked by impaired proliferative capacity and reduced effector functions[19]. To delineate the dynamic changes in T-cell states during tumor progression, we isolated TILs from MC38 tumor-bearing mice at an advanced stage (day 19 post-inoculation) and performed single-cell RNA sequencing (scRNA-seq) on $CD8^+$ T cells. The MC38 murine colon adenocarcinoma cell line, established in 1975 from a chemically induced tumor in female C57BL/6 mice, is a widely used model in cancer research and therapy development[20]. Our analysis revealed four distinct states of intratumoral $CD8^+$ T cells (Fig. 1A). A subset of proliferating $CD8^+$ T cells was identified by high Ki67 expression and low levels of exhaustion markers including *Pdcd1* and *Havcr2*. In contrast, $CD8^+$ T cells in the exhausted state displayed elevated levels of *Pdcd1* and *Havcr2* without *Ki67* expression, suggesting a loss of proliferative potential (Fig. 1B, C). To further demonstrate human relevance, we analyzed published scRNA-seq data from human colorectal cancer (CRC) samples[21]. As shown below, $TIM3^+CD8^+$ T cells from human CRC tumors also showed higher expression of exhaustion-related genes (*ENTPD1*, *PDCD1*, *HAVCR2*) but lower function and proliferation-related genes (*GZMK*, *GZMH*, *TNF*, *KLRG1*, *MKI67*), indicating that these cells are exhausted (Supplementary Fig. 1A–C).

To directly assess whether tumor-specific $CD8^+$ T cells predominantly adopt an exhausted state within the TME, we employed Tetramer-based tracking of tumor-specific T cells in the MC38-OVA tumor model. Our findings revealed that more than 80% of Tetramer-positive $CD8^+$ T cells co-expressed TIM3, confirming that tumor-specific T cells are largely exhausted (Fig. 1D, Supplementary Figs. 2, 4A). Further flow cytometry analysis confirmed that $TIM3^+$ $CD8^+$ T cells co-express established exhaustion markers such as PD-1, CD39 and LAG3, supporting their classification as exhausted T cells based on this multi-marker profile (Supplementary Fig. 3A–D). The scRNA-seq analysis revealed reduced *Bcl2* expression in exhausted T cells (Fig. 1B, C). Consistently, flow cytometry analysis demonstrated decreased Bcl-2 levels in $TIM3^+CD8^+$ T cells compared to $TIM3^-CD8^+$ T cells (Fig. 1E and Supplementary Fig. 4B), indicating an enhanced susceptibility to apoptosis. These observations underscored the critical need to develop strategies to reactivate exhausted T cells.

To reactivate T cells, the cross presentation of DC cells is required. However, we found that tumor-infiltrating DC (TIDC) exhibited impaired ability to prime cytotoxic $CD8^+$ T cells (Fig. 1F, G and Supplementary Fig. 4C). As is well known, IFNα has been shown to amplify DC activation, prompting us to investigate whether IFNα could enhance DC-T cell crosstalk in the TME to reactivate exhausted T cells. Analysis of clinical RNA-seq data from the KM plotter database (including lung cancer and colorectal adenocarcinoma cohorts) revealed that suppressed IFN-α signaling and high TIM3 expression are both associated with poor survival (Supplementary Fig. 4D, E). GSEA analysis of interferon alpha/beta signaling genes in ICB responsive compared with ICB non-responsive melanoma patients, and found that interferon alpha/beta signaling genes are enriched in ICB responsive melanoma patients (Supplementary Fig. 4F), indicating that IFN-I signaling is important for the therapeutic effects of ICB[22,23].

Since monotherapies targeting TIM3 or IFNα showed limited efficacy in advanced tumors[6,14,24], we proposed that targeting TIM3-positive cells with IFN could overcome such resistance by a combinatorial strategy. Strikingly, dual intraperitoneal administration of anti-TIM3 and Fc-IFNα additively improved therapeutic outcomes (Fig. 1H). However, even with this enhanced response, the combination failed to achieve complete eradication of established tumors but also caused severe toxicity (Fig. 1I), highlighting the need for further optimization. Collectively, our data suggested that combining IFN-I with TIM3 blockade additively enhanced control of advanced tumors.

BiDT elicits potent antitumor immunity in vivo

Given the superior antitumor efficacy of combined anti-TIM3 and IFNα therapy compared to monotherapies but severe IFNα-mediated toxicity (Fig. 1H, I), we need to reduce IFNα-associated toxicity while increasing tumor targeting. To achieve targeted delivery of IFNα to the TME, we adopted an antibody-based strategy, specifically using an anti-TIM3 antibody. Initial analysis in MC38 tumor-bearing mice confirmed that TIM3 expression was significantly higher on $CD45^+$ immune cells within established tumors compared to those in the TDLNs of mice with advanced cancer (Supplementary Fig. 5A). This elevated and localized expression profile supported the rationale that a TIM-3-directed approach could facilitate the specific transport of IFN-α to the TME[25]. Moreover, we further assessed the expression on multiple immune cells within the TME, finding the significantly highest level of TIM3 on $CD8^+$ T cells, compared to it on DC and $CD4^+$ T cells (Supplementary Fig. 5B). We proposed to use the high affinity of anti-TIM3 antibody to guide IFNα.

Concurrently, to enhance tumor-specific targeting and mitigate potential systemic toxicity, we needed to screen an IFNα fusion protein structure with lower IFNAR receptor affinity. This design aimed to ensure that the IFNα payload would be preferentially localized within the TME upon targeted delivery by the TIM3 antibody, rather than exerting effects in the periphery. To this end, we designed and compared two distinct architectures for the TIM3 antibody-IFNα fusion protein: a heterodimer format and a homodimer format (Fig. 2A). Subsequent evaluation aimed to identify the construct possessing the lower IFNα binding affinity for further development. In IFNAR-expressing $TIM3^-$ cells, the heterodimer format exhibited significantly reduced binding of IFNα to IFNAR compared to the homodimer (Supplementary Fig. 5C). Based on these findings, the heterodimeric anti-TIM3-IFNα fusion protein (TIM3-IFNα) was selected as the lead construct, ensuring targeted delivery and localized

https://doi.org/10.1038/s41467-026-70876-4

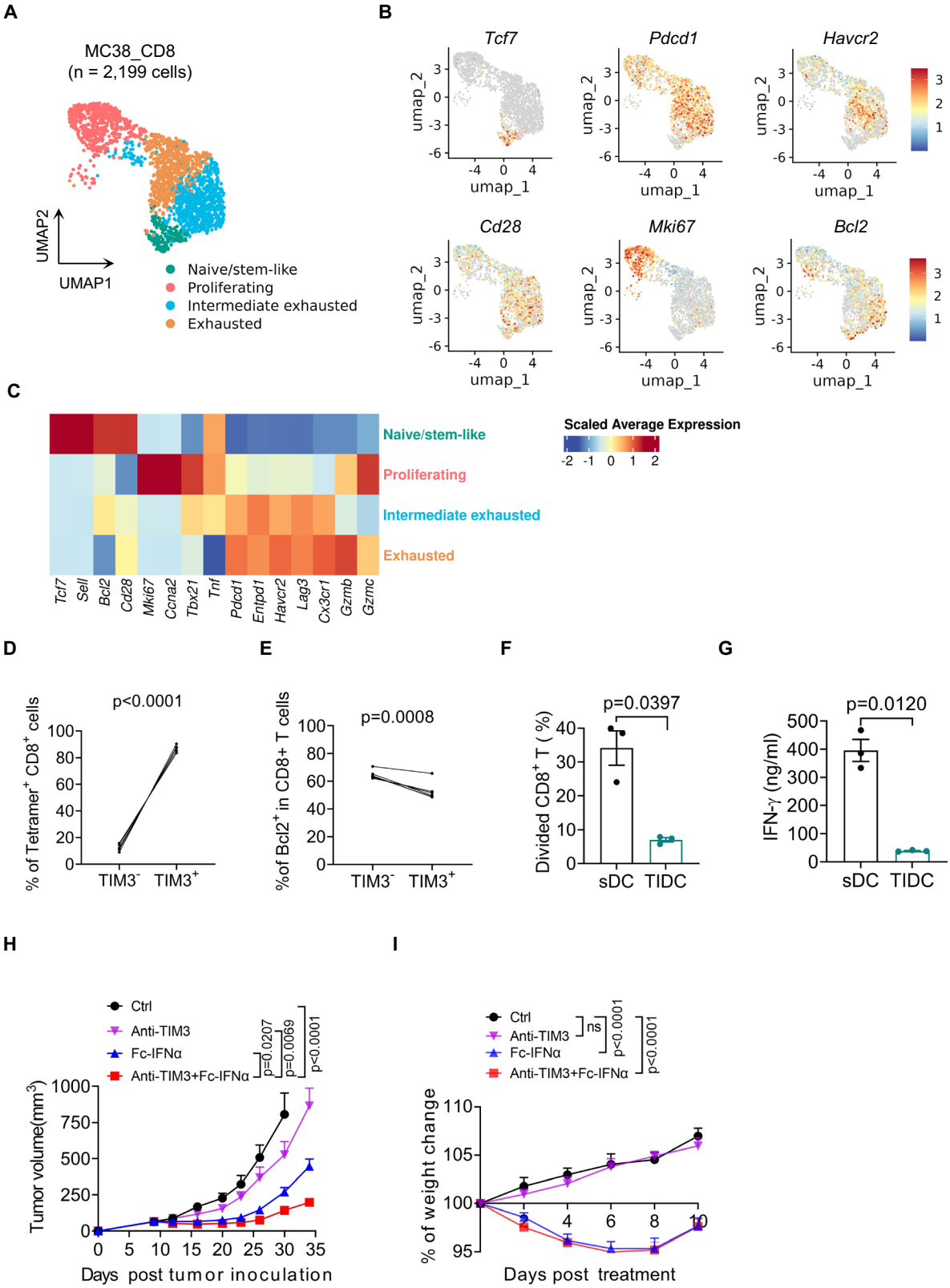

activation of IFNα within the TME via the TIM3 antibody. This bispecific reagent is also engineered to concurrently target the immune checkpoint TIM3 on exhausted TILs and engage DC via the IFNAR, thereby facilitating the reactivation of exhausted tumor-reactive T cells through bispecific dendritic cell-T cell engagement (BiDT).

To evaluate the tumor-targeting efficacy of this designed BiDT, we conjugated it with a Cy5-maleimide tracer and administered it to tumor-bearing mice for whole-body imaging. Bioluminescence imaging revealed robust and specific accumulation of BiDT within tumor tissues (Supplementary Fig. 6A, B), confirming its targeted delivery to the TME and decreased the peripheral toxicity (Fig. 2B). Impressively, the systemic delivery of low-dose BiDT in MC38 tumor-bearing mice enhances antitumor efficacy, resulting in complete tumor eradication among most murine subjects. In contrast, the combination of anti-

Fig. 1 | Tumor-reactive T cells are exhausted inside advanced tumors. **A**–**C** Female C57BL/6 mice ($n = 5$) were inoculated with 5×10^5 MC38 cells. $CD8^+$ T cells were sorted for single-cell RNA sequencing 19 days after tumor inoculation. **A** UMAP plot of 2276 $CD8^+$ T cells exhibiting four cell subsets. **B** Expression of selected markers among $CD8^+$ T cells by 2D UMAP visualization. **C** Heatmap plot showing average relative expression of selected markers in four $CD8^+$ T cell subsets. **D** Female C57BL/6 mice ($n = 6$) were inoculated with 1×10^6 MC38-OVA cells. The tumor tissues were collected 19 days after tumor inoculation. TIM3 expressions on $Tetramer^+CD8^+$ T cells in tumors from MC38-OVA tumor-bearing mice. **E** Female C57BL/6 mice ($n = 6$) were inoculated with 5×10^5 MC38 cells. The tumor tissues were collected 19 days after tumor inoculation. Bcl-2 expressions on $TIM3^-CD8^+$ T cells or $TIM3^+CD8^+$ T cells in tumors from MC38 tumor-bearing mice. The proliferation and function of OT-I $CD8^+$ T cells primed by spleen DC (sDC) or TIDC ($n = 3$/group) were assessed using CFSE dilution (**F**) and IFN-γ production (**G**). **H**, **I** MC38-bearing Female C57BL/6 mice ($n = 7$/group) were i.p. treated with 200 μg anti-TIM3 and/or 25 μg Fc-IFNα on day 9, 12 and 15 after tumor inoculation. Tumor volume (**H**) and mice weight (**I**) were measured as indicated. Data are shown as mean ± SEM and are representative of at least two independent experiments. *P* value was determined by paired two-tailed *t* tests (**D**, **E**), unpaired two-tailed *t* tests (**F**, **G**) or One-way ANOVA with Tukey's test (**H**, **I**). Source data are provided as a Source Data file.

TIM3 and Fc-IFNα failed to achieve comparable antitumor effects (Fig. 2C). Notably, BiDT treatment significantly improved overall survival compared to combination therapy (Fig. 2D). Together, these results suggest that BiDT's efficacy has a synergistic effect for enhancing efficacy while reducing toxicity.

We wonder whether such DC-T cell interaction inside TME can also generate more tumor-specific memory T cells for systemic protection. To test that, we harvested the splenocytes from mice 15 days after treatment. Indeed, we observed BiDT-induced robust antigen-specific memory T-cell responses that moved to the periphery, as evidenced by increased tumor-specific IFN-γ-producing cells in the spleen of tumor-bearing mice (Fig. 2E and Supplementary Fig. 6C). Accordingly, we performed surface staining for memory markers on splenocytes. Our analysis revealed a significant increase in the proportion of central memory T cells within the splenocyte population following BiDT treatment (Supplementary Fig. 7A, B). Recognizing the importance of memory T-cell responses for long-term immunity[26], we rechallenged BiDT-cured mice with a fourfold higher tumor cell dose 50 days post-treatment. The absence of tumor growth confirmed the induction of effective and prolonged memory responses (Fig. 2F). Furthermore, the adoptive transfer of splenocytes from tumor-cured mice into *Rag1*$^{-/-}$ recipients resulted in tumor rejection (Fig. 2G), further validating the role of memory T cells in enhancing tumor surveillance and efficiently recognizing and eliminating tumor cells. Lastly, to assess the impact on metastasis formation, a major cause of cancer mortality[27], we utilized a pulmonary metastasis model. Mice bearing subcutaneous B16F10 tumors received an intravenous injection of additional B16F10 cells one day prior to low dose of BiDT treatment (Fig. 2H). Intratumoral BiDT administration significantly delayed local tumor growth (Fig. 2I) and suppressed lung metastasis formation (Fig. 2J and Supplementary Fig. 6D). Collectively, these findings indicate that BiDT induces a robust tumor-specific immune response to eradicate primary tumors and generate memory responses, which is capable to suppress metastasis and prevent recurrence.

Pre-existing CD8 T cells and DC are essential and sufficient for the antitumor effect of BiDT

TIM3 and IFNAR are widely expressed on immune cells, with type I IFNs in particular acting as versatile cytokines that bridge innate and adaptive immunity[28,29]. To fully understand the mechanism of BiDT, it is essential to identify which immune cells are involved in the treatment and determine the specific roles of TIM3 and IFNAR on these cells. Initial studies in *Rag1*$^{-/-}$ mice, which lack adaptive immunity but have enhanced NK cell activity[30], revealed a complete abrogation of BiDT's antitumor effects, highlighting the pivotal contribution of the adaptive immunity in mediating therapeutic efficacy (Fig. 3A). To delineate the contribution of distinct T cell subsets to the therapeutic effect of BiDT, we performed depletion experiments using anti-CD4 or anti-CD8 antibodies. These studies revealed that the depletion of $CD8^+$ T cells, but not $CD4^+$ T cells, abrogated the therapeutic efficacy of BiDT (Fig. 3B). To assess the contributions of innate immune cells, we depleted NK cells by anti-NK1.1 and macrophages by anti-CSF1R in WT mice[31]. Neither depletion impaired BiDT's efficacy, indicating that these cell types are dispensable for its antitumor effects (Fig. 3C). Given the established role of DC in mediating type I IFN responses, we next evaluated their contribution to BiDT therapy. Using CD11c-DTR chimeric mice inoculated with MC38 tumors, we observed that DC depletion via diphtheria toxin (DT) completely abolished BiDT's therapeutic effects, confirming the necessity of DC (Fig. 3D, E). These findings highlight the critical role of $CD8^+$ T cells and DC in mediating the therapeutic effects of BiDT.

To investigate whether the therapeutic efficacy of BiDT relies on the continuous influx of T cells or preexisting T cells within the TME, we used FTY720, a compound that blocks T cell egress from lymph nodes, rapidly diminishing circulating T cells and halting their recruitment into tumors during treatment[32]. Results demonstrated that FTY720 did not compromise BiDT's antitumor efficacy (Fig. 3F), indicating that preexisting T cells in the TME were sufficient to mediate tumor control. To further validate this conclusion, we conducted tumor transfer experiments: MC38 tumor tissues from wild-type mice were transplanted subcutaneously (s.c.) into *Rag1*$^{-/-}$ mice (which lack mature lymphocytes) and intratumoral injected with BiDT. In this model, all T cells present were derived exclusively from the transferred tumor tissue, excluding contributions from recipient lymph nodes. This approach corroborated that preexisting intratumoral T cells alone could drive BiDT's therapeutic effect (Fig. 3G). Combined with the previously mentioned dominant roles of T cells and dendritic cells in the immune response, the data further suggest BiDT treatment relies on intratumoral DC and T cells. Collectively, these results pinpoint preexisting $CD8^+$ T cells, and DC are essential and sufficient for the antitumor effect of BiDT.

BiDT treatment enhances the crosstalk between DC and $TIM3^+$ T cells

To dissect the contribution of IFNAR signaling in different cell populations to BiDT's therapeutic efficacy[33], we conducted a series of knockout (KO) experiments. Initially, to assess the impact of IFNAR signaling in tumor cells on BiDT-mediated antitumor activity, we evaluated its therapeutic efficacy in mice bearing *Ifnar1*$^{-/-}$ MC38 tumors. BiDT retained its antitumor activity in mice bearing *Ifnar1*$^{-/-}$ MC38 tumors, whereas its efficacy was completely abrogated in *Ifnar1*$^{-/-}$ mice harboring WT MC38 tumors (Fig. 4A, B). These findings indicated that IFNAR signaling in host cells, rather than tumor cells, is essential for the antitumor effects of BiDT. Next, we investigated the necessity of IFNAR signaling in $CD8^+$ T cells for the efficacy of BiDT therapy. We adoptively transferred sorted WT or *Ifnar1*$^{-/-}$ $CD8^+$ T cells into tumor-bearing *Rag1*$^{-/-}$ mice and treated them with BiDT. Notably, BiDT continued to inhibit tumor growth even in the absence of IFNAR signaling in $CD8^+$ T cells, indicating that IFNAR expression on T cells is not required for the therapeutic effects of this BiDT therapy (Fig. 4C, D). To further clarify the role of IFNAR expression in DC within the TME, we conditionally deleted IFNAR in dendritic cells (*Zbtb46*-Cre *Ifnar1* $^{fl/fl}$). The therapeutic efficacy of BiDT was lost in mice with DC-specific IFNAR knockout (Fig. 4E). Together, our experiments highlight the importance of IFNAR on DC for the treatment of BiDT.

https://doi.org/10.1038/s41467-026-70876-4

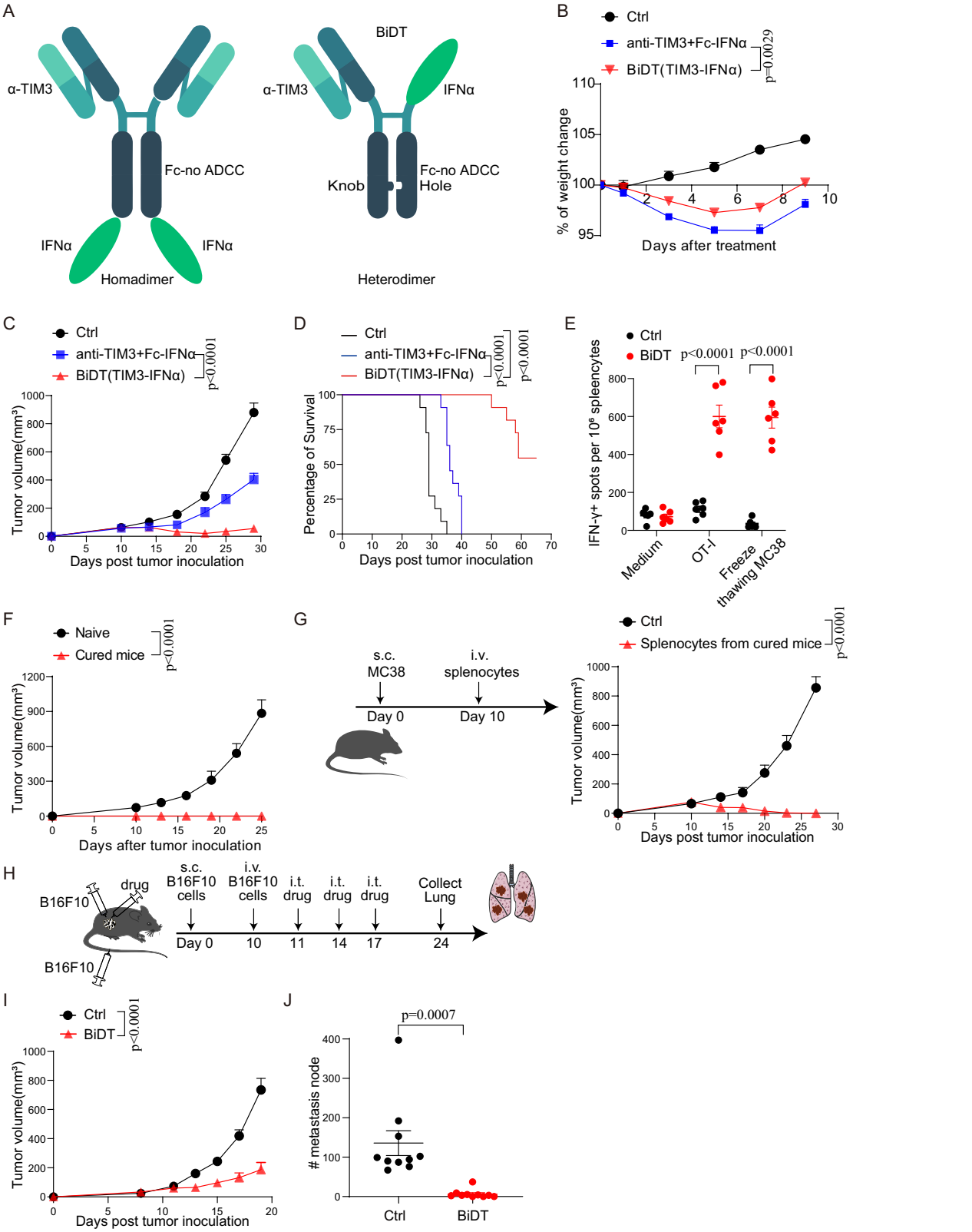

TIM3 is expressed on T cells as well as myeloid cells[34]. To further delineate the function of TIM3 in different immune cell populations, we specifically deleted TIM3 in DC (*Zbtb46*-Cre *Havcr2*$^{fl/fl}$), macrophages (*Lyz2*-Cre *Havcr2*$^{fl/fl}$), or T cells (*Cd4*-Cre *Havcr2*$^{fl/fl}$). We observed that BiDT retained its therapeutic efficacy in mice lacking TIM3 on DC and macrophages but not in mice harboring T cell-specific TIM3 deletion (Fig. 4F, G), demonstrating that TIM3 engagement on T cells, but not myeloid cells, is critical for BiDT's antitumor activity. Further validating these findings, we investigated CD8$^+$ T-cell dynamics in the MC38 tumor model. Treatment with BiDT resulted in a significant expansion of CD8$^+$ T cells within the TME (Fig. 4H). Further analysis revealed that this increase was primarily driven by TIM3$^+$CD8$^+$ T cells, with no notable change in the TIM3$^-$CD8$^+$ T cell population (Fig. 4H and Supplementary Fig. 8A). Similar trends were observed in tumor-

Fig. 2 | BiDT generates potent antitumor immunity. A Schematic diagram of TIM3-IFNα fusion protein in homodimer or heterodimer format. **B**–**D** MC38 tumor-bearing female C57BL/6 mice ($n = 11$/group) were i.p. treated with BiDT (25 μg), or a mixture of Fc-IFNα and anti-TIM3 (12.5 μg + 12.5 μg), on day 13, 16 and 19 post inoculation. Mice weight (**B**) and tumor volume (**C**) were measured as indicated and the corresponding mouse survival curve was shown in (**D**). **E** MC38-OVA tumor-bearing female C57BL/6 mice ($n = 6$/group) were i.p. treated with 25 μg BiDT on day 13, 16 and 19 post inoculation. At day15 after treatment, splenocytes from different treatment groups were isolated and stimulated with either OT-I peptide or freeze-thawing MC38-OVA tumor cells. Antigen-specific T cells were detected by ELISpot assay. The splenocyte quantification data are shown in (**E**). **F**, **G** MC38-bearing female C57BL/6 mice were i.p. treated with 25 μg BiDT on day 13, 16 and 19 post inoculation. At 15 day after treatment, cured mice ($n = 5$/group) were re-challenged with 2×10^6 MC38 tumor cells (**F**), 2×10^7 splenocytes from cured mice were i.v. transferred to MC38-bearing *Rag1*$^{-/-}$mice ($n = 5$/group) 10 days after inoculation (**G**). Tumor volume was measured as indicated. **H**–**J** Female C57BL/6 mice ($n = 10$/group) were subcutaneously inoculated with 3×10^5 B16F10 tumor cells and injected with 2×10^6 B16F10 tumor cells through the tail vein on day 10. The subcutaneous tumor was intratumorally treated with 5 μg BiDT on days 11, 14, and 17. The mice were euthanized on day 21 post inoculation. The lungs were collected (**H**). The subcutaneous B16F10 tumor growth curve (**I**). The number of B16F10 tumor metastatic nodes in the lung (**J**). Data are shown as mean ± SEM and are representative of at least two independent experiments. *P* value was determined by One-way ANOVA with Tukey's test (**B**, **C**) or unpaired two-tailed *t* tests (**E**–**G**, **I**, **J**). Survival curve was compared using the log-rank test (**D**). Source data are provided as a Source Data file.

specific CD8$^+$ T cells. In the MC38-OVA model, BiDT treatment led to a marked increase in Tetramer$^+$CD8$^+$ T cells within the TME (Fig. 4I). This expansion was predominantly attributed to TIM3$^+$Tetramer$^+$CD8$^+$ T cells, while the TIM3$^-$Tetramer$^+$CD8$^+$ T cell population remained largely unchanged (Fig. 4I and Supplementary Fig. 8B). These data confirmed the necessity of TIM3 expression on T cells for the anti-tumor effects of BiDT.

Collectively, these results establish that BiDT mediates its therapeutic effects primarily through IFNAR signaling in DC and TIM3 engagement on CD8$^+$ T cells, providing a mechanistic basis of close DC-T interaction for reactivating TILs inside the TME, an important but previously difficult testing issue in cancer immunotherapy.

BiDT reactivates exhausted CD8$^+$ TILs into a more effector-like state

To assess the functional impact of BiDT on TILs, we isolated intratumoral CD8$^+$ T cells and performed single-cell RNA sequencing three days post-BiDT treatment (Fig. 5A). Our analysis revealed four distinct states of CD8$^+$ T cells. Following BiDT monotherapy, the proportion of CD8$^+$ T cells in the exhausted state was significantly reduced, while the proportion of CD8$^+$ T cells in an effector-like exhausted state markedly increased (Fig. 5B, C). These phenotypically exhausted CD8$^+$ T cells now exhibited elevated expression of genes associated with pro-inflammatory cytokines and cytokine receptors, including *Ifng, Gzmb, Fasl, Il2ra*, and *Il10ra*, as well as costimulatory molecules such as *Cd28* and inhibitory receptors, compared to the exhausted counterparts (Fig. 5D, E). These findings suggest that BiDT reprogrammed exhausted CD8$^+$ TILs into a more functional state. To further validate this hypothesis, we sorted and analyzed TIM3$^+$ exhausted CD8$^+$ T cells by flow cytometry 20 h post-BiDT treatment. These cells displayed increased expression of pro-inflammatory cytokines and cytokine receptors, including IFN-γ, GZMB, IL-2, and CD25 (Fig. 5F and Supplementary Fig. 9A–D). Given the short timeframe for fusion protein moving into the TME to push the transcription and translation of those effector molecules, it is unlikely that these effector-like exhausted CD8$^+$ T cells proliferated and differentiated from other subsets, supporting the notion that BiDT reactivates exhausted CD8$^+$ TILs.

Gene set enrichment analysis (GSEA) showed the enrichment of the genes associated with the T cell receptor signaling pathway and the IL-2/STAT5 signaling pathway in effector-like exhausted CD8$^+$ T cells (Fig. 5G), indicating that their enrichment is dependent on these signaling pathways. Collectively, these results suggest that BiDT reprograms exhausted CD8$^+$ TILs into a more functional state, enhancing their capacity to mediate antitumor immunity.

Co-stimulatory and IL-2 signaling are essential for BiDT-mediated antitumor effects

To study how BiDT enhances DC function, we explored the potential key molecules on DC that are important for activating TILs. Our data showed that BiDT treatment significantly increased DC activation, as evidenced by elevated CD80 and CD86 expression (Fig. 6A, Supplementary Fig. 10A–C, and Supplementary Fig. 13A). We hypothesized that the therapeutic efficacy of BiDT relies on CD28-mediated T cell co-stimulation provided by CD80/86 interactions through DC-T cell crosstalk. To test this, we combined BiDT with anti-CD80/86 antibodies to block CD80/86-CD28 co-stimulation. Strikingly, this blockade completely abolished the antitumor effects of BiDT (Fig. 6B), underscoring the essential role of co-stimulatory signaling from DC to T cells in BiDT-mediated therapy.

Previous studies have demonstrated that CD28 co-stimulation enhances T-cell survival by inhibiting apoptosis and increasing the number of TILs[11]. We hypothesized that BiDT might similarly suppress apoptosis in exhausted T cells, thereby expanding TILs and tumor-specific T cells through CD80/86-CD28 co-stimulation. Single-cell RNA sequencing data revealed that BiDT upregulated *Bcl2* expression in CD8$^+$ T cells (Supplementary Fig. 11). Consistent with this, we observed a reduction in active caspase-3, a marker of apoptosis, and an increase in the anti-apoptotic protein Bcl-2 in exhausted T cells following BiDT treatment, indicating its anti-apoptotic effects (Fig. 6C, D and Supplementary Fig. 12A, B). Notably, the blockade of CD28 co-stimulation abrogated the anti-apoptotic function of BiDT (Fig. 6C, D and Supplementary Fig. 12A, B), highlighting the essential role of co-stimulatory signaling in BiDT-mediated therapy.

Analysis of the Cancer Genome Atlas (TCGA) database for clinical data revealed that DC infiltration and CD80/86 expression significantly correlated with the level of CD25 (Supplementary Fig. 13D, E). As well known, CD25 is not only a marker of T cells but also a critical component of the IL-2 receptor (IL-2R)[35,36]. Further investigation into T cell activation and differentiation revealed that BiDT treatment induced higher expression of CD25 on TILs (Fig. 6E and Supplementary Fig. 12C). Blockade of CD80/86-CD28 co-stimulation reduced CD25 expression to baseline levels, indicating that BiDT-induced CD25 upregulation is dependent on co-stimulatory signaling (Fig. 6E). Higher CD25 expression correlates with the formation of high-affinity trimeric IL-2 receptor[36,37], suggesting that BiDT might enhance the responsiveness of T cells to endogenous or exogenous IL-2. To test that, additional IL-2 overcame the resistance and achieved complete elimination of the more advanced tumors (Supplementary Fig. 13B, C), highlighting the synergistic role of IL-2 signaling in enhancing the antitumor efficacy of BiDT. Previous GSEA also highlighted the importance of IL-2 signaling in reprogramming exhausted CD8$^+$ TILs into a more functional state. Therefore, we proposed that the antitumor effect of BiDT depended on the IL-2 signal pathway. BiDT restored IL-2 production in exhausted CD8$^+$ T cells (Fig. 6F and Supplementary Fig. 12D). Blocking CD80/86-CD28 co-stimulation not only reduced CD25 expression but also decreased IL-2 production (Fig. 6E, F).

IL-2 stimulation could trigger CD8$^+$ T cells to produce antitumor cytokines such as IFN-γ[19,38]. BiDT monotherapy also enhanced the IFN-γ production of exhausted TILs (Fig. 6G and Supplementary Fig. 12E).

https://doi.org/10.1038/s41467-026-70876-4

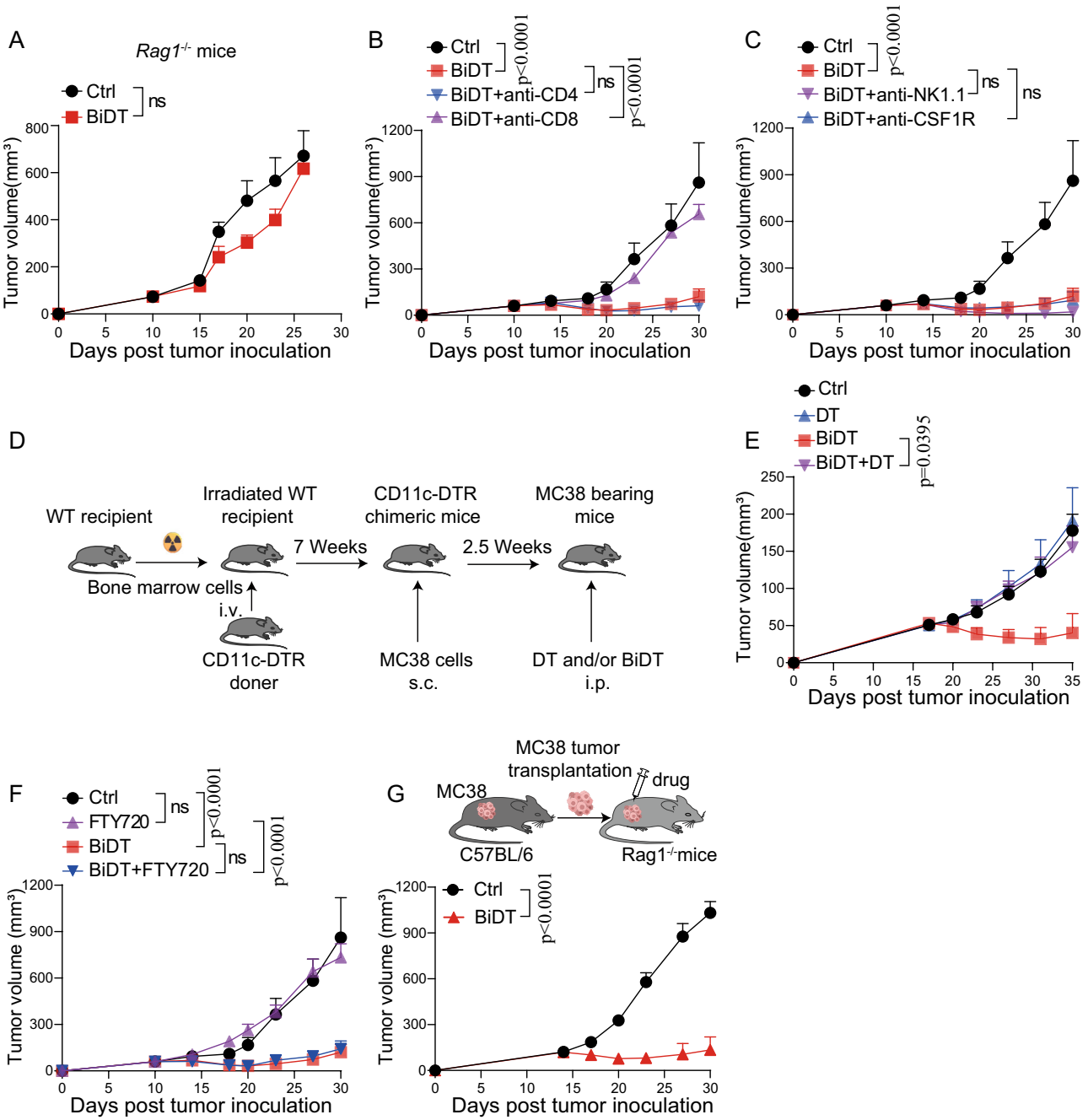

Fig. 3 | Preexisting CD8⁺ T cells and DCs are essential and sufficient for the antitumor effect of BiDT. A MC38-bearing female *Rag1*$^{-/-}$ mice ($n = 6$/group) were i.p. treated with 25 μg BiDT on day 13, 16 and 19 after tumor inoculation. Tumor volume was measured as indicated. **B** MC38-bearing female C57BL/6 mice ($n = 7$/group) were i.p. treated with 25 μg BiDT on day 13, 16 and 19 after tumor inoculation. Anti-CD4 or anti-CD8 was administrated twice a week for 2 weeks. Tumor volume was measured as indicated. **C** MC38-bearing female C57BL/6 mice ($n = 7$/group) were i.p. treated with 25 μg BiDT on day 13, 16 and 19 after tumor inoculation. Anti-CSF1R or anti-NK1.1 was administrated twice a week for 2 weeks. **D**, **E** Female C57BL/6 mice were lethally irradiated (10 Gy). Bone marrow was isolated from CD11c-DTR donor mice. Irradiated C57BL/6 mice as recipient were i.v. transferred with 2×10^6 CD11c-DTR bone marrow cells. CD11c-DTR chimeric mice were rested for 7 weeks and then were inoculated with MC38 cells. MC38-bearing CD11c-DTR chimeric mice ($n = 5$/group) were i.p. treated with 25 μg BiDT on day 18, 21 and 24 after tumor inoculation. DT was administrated at 200 ng two days before treatment initiation and then every other day for 2 weeks (**D**). Tumor volume was measured as indicated (**E**). **F** MC38-bearing female C57BL/6 mice ($n = 7$/group) were i.p. treated with 25 μg BiDT on day 13, 16 and 19 after tumor inoculation. FTY720 was administrated at 20 μg every other day for 2 weeks. **G** Female C57BL/6 mice were inoculated with 5×10^5 MC38 cells. The mice were euthanized on day 16 after tumor inoculation. 120 mm^3 MC38 tumor tissues were collected and s.c. transferred to *Rag1*$^{-/-}$ mice ($n = 6$/group). The subcutaneous tumor was intratumorally treated with 25 μg BiDT on days 0, 3, and 6 after tumor transplanting. Data are shown as mean ± SEM and are representative of at least two independent experiments. *P* value was determined by One-way ANOVA with Tukey's test (**B**, **C**, **E**, **F**) or unpaired two-tailed *t* tests (**A**, **G**). Source data are provided as a Source Data file.

Administration of an anti-CD80/86 blocking antibody in combination with BiDT resulted in a significant reduction in IFN-γ production (Fig. 6G). We proposed that BiDT reactivates TILs, leading to increased production of cytokines, particularly IFN-γ, by enhancing the IL-2 signaling pathway in TILs through CD80/86-CD28 co-stimulation. Notably, IFN-γ was highly produced in CD25⁺CD8⁺ T cells (Supplementary Figs. 12F, 13F), suggesting that IL-2 signaling reactivates exhausted TILs and enhances their cytokine production. To validate

https://doi.org/10.1038/s41467-026-70876-4

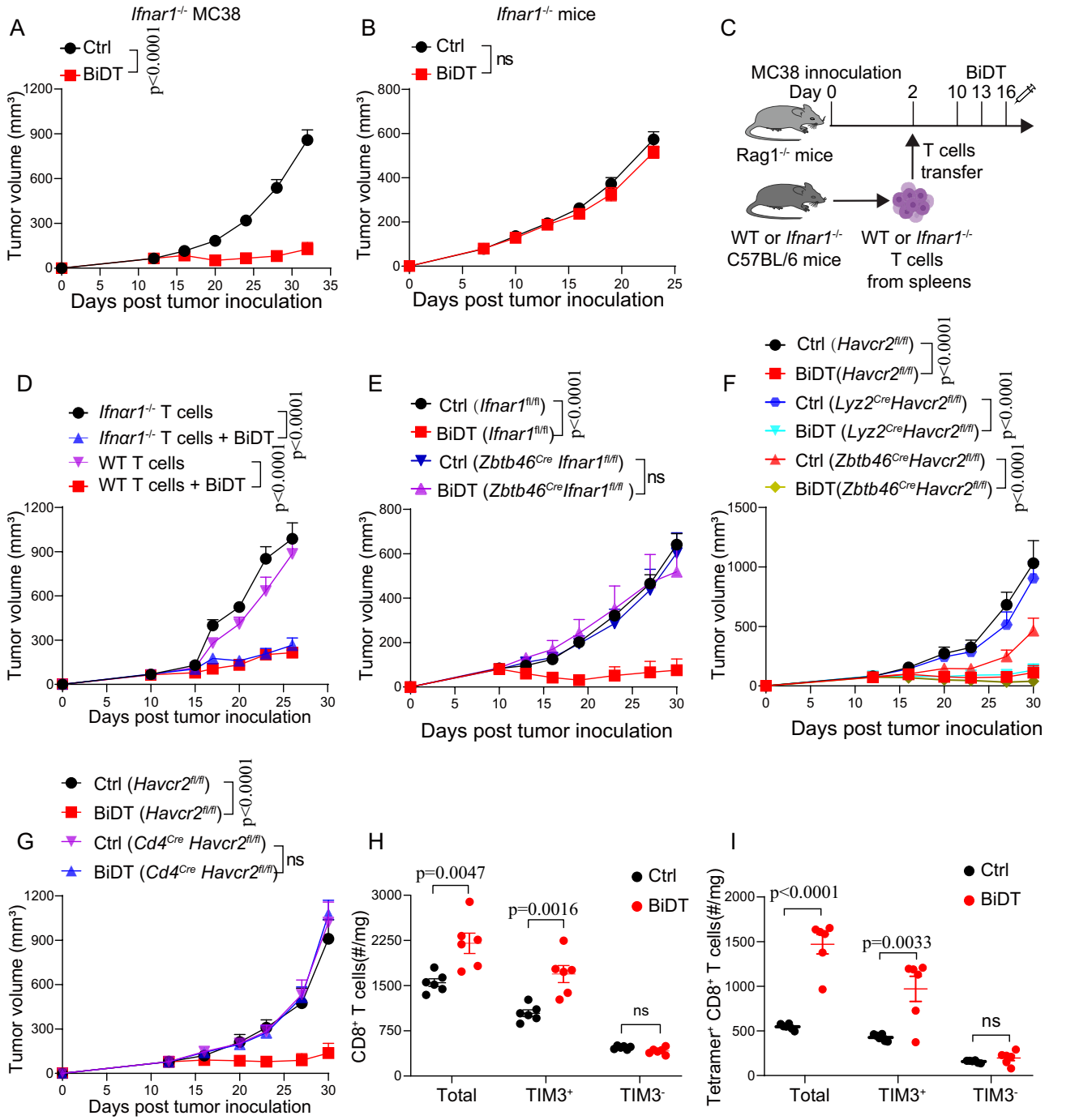

Fig. 4 | BiDT treatment enhances the crosstalk between DCs and TIM3⁺ T cells. **A** Female C57BL/6 mice ($n = 6$/group) were inoculated with 1×10^6 *Ifnar1*$^{-/-}$MC38 cells and treated with 25 μg BIDT on day 13, 16 and 19 after tumor inoculation. Tumor volume was measured as indicated. **B** MC38-bearing female *Ifnar1*$^{-/-}$ mice ($n = 6$/group) were i.p. treated with 25 μg BiDT on day 10, 13 and 16 after tumor inoculation. **C**, **D** 3×10^6 CD3⁺ T cells from spleen of female C57BL/6 mice or *Ifnar1*$^{-/-}$ mice were adoptively transferred to MC38-bearing *Rag1*$^{-/-}$ mice ($n = 6$/group) 2 days after tumor inoculation. 25 μg BiDT was i.p. administrated on day10, 13 and 16 after tumor inoculation (**C**). Tumor volume was measured as indicated (**D**). **E** Female *Ifnar1*$^{fl/fl}$ mice and *Zbtb46-Cre Ifnar1*$^{fl/fl}$ mice ($n = 8$/group) were inoculated with 5×10^5 MC38 tumor cells and i.p. treated with 25 μg BiDT on day 13, 16 and 19 after tumor inoculation. **F** Female *Havcr2*$^{fl/fl}$ mice, *Zbtb46-Cre Havcr2*$^{fl/fl}$ mice or *Lyz2-Cre Havcr2*$^{fl/fl}$ mice ($n = 6$/group) were inoculated with 5×10^5 MC38 tumor cells and i.p. treated with 25 μg BiDT on day 13, 16 and 19 after tumor inoculation. **G** Female *Havcr2*$^{fl/fl}$ mice or *Cd4-Cre Havcr2*$^{fl/fl}$ mice ($n = 6$/group) were inoculated with 5×10^5 MC38 tumor cells and i.p. treated with 25 μg BiDT on day 13, 16 and 19 after tumor inoculation. **H** MC38-bearing female C57BL/6 mice ($n = 6$/group) were treated with 25 μg BiDT on day 16. Tumor tissues were collected 72 h after injection. The number of intratumoral total CD8⁺T cells/TIM3⁺CD8⁺T cells and TIM3⁻CD8⁺T cells (**H**) were measured by FACS. **I** MC38-OVA tumor-bearing female C57BL/6 mice ($n = 6$/group) were treated with 25 μg BiDT on day 16. Tumor tissues were collected 72 h after injection. The number of total Tetramer⁺, TIM3⁺Tetramer⁺CD8⁺ T cells and TIM3⁻Tetramer⁺CD8⁺ T cells (**I**) were measured by FACS. Data are shown as mean ± SEM and are representative of at least two independent experiments. *P* value was determined by unpaired two-tailed *t* tests (**A**, **B**, **H**, **I**) or One-way ANOVA with Tukey's test (**D**–**G**). Source data are provided as a Source Data file.

https://doi.org/10.1038/s41467-026-70876-4

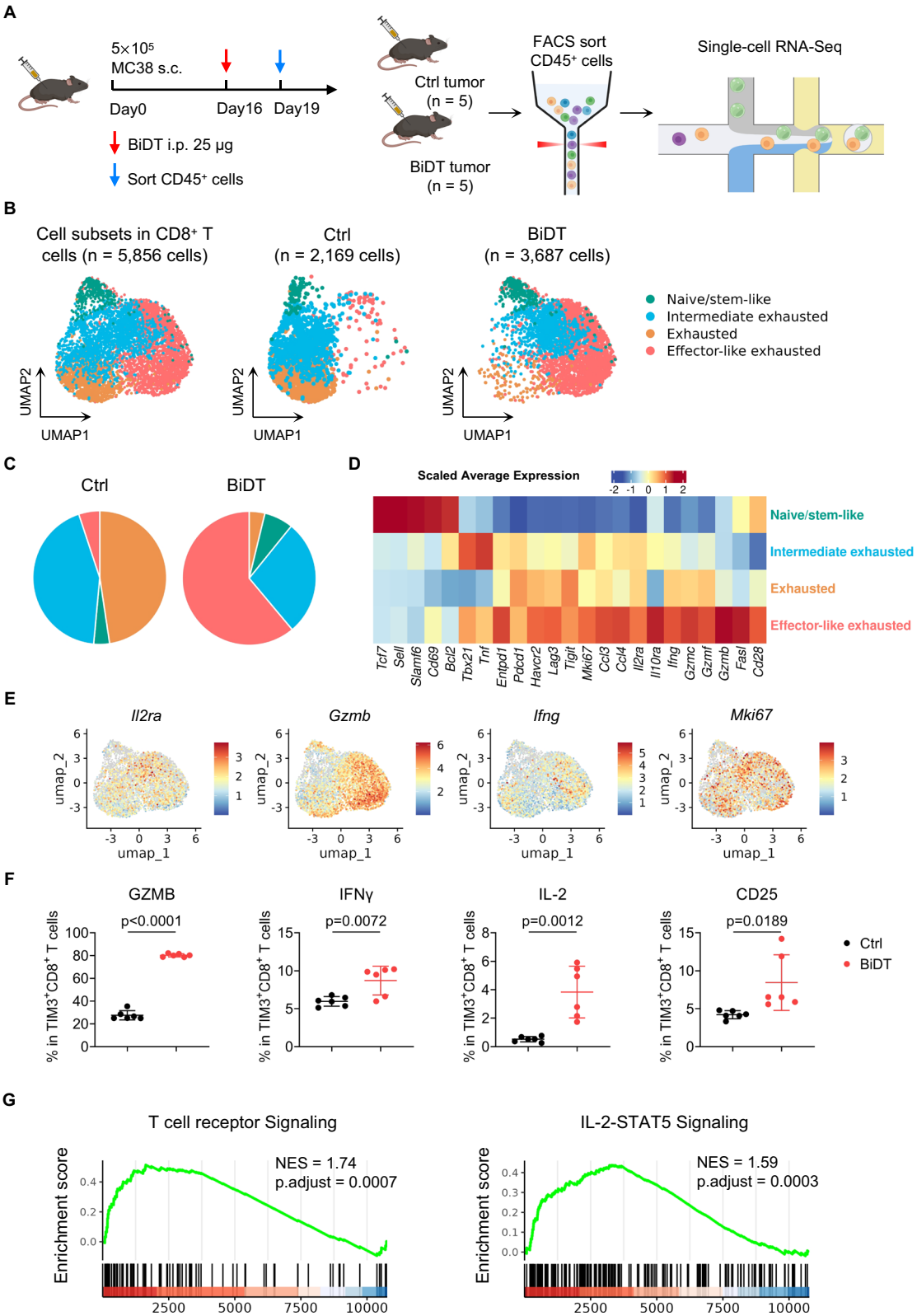

Fig. 5 | BiDT reactivated exhausted CD8⁺ TILs into more effector-like exhausted CD8⁺ TILs. A The experimental scheme. **B** UMAP plot of 5856 CD8⁺ T cells showing four cell subsets (2169 cells from PBS treated group and 3689 cells from BiDT-treated group). **C** Cell compositions of CD8⁺ T cell subsets from PBS and BiDT-treated group. **D** Heatmap plot showing average relative expression of selected genes across four CD8⁺ T cell subsets depicted in (**B**). **E** Expression of selected markers among CD8⁺ T cells via 2D UMAP visualization. **F** Proportions of GZMB⁺, IFNγ⁺, IL-2⁺ and CD25⁺ cells ($n = 6$/group) within TIM3⁺CD8⁺ TILs measured by flow cytometry. **G** Gene set enrichment analysis of T cell receptor signaling and IL-2-STAT5 signaling genes in effector-like exhausted TILs compared with exhausted TILs. Data are shown as mean ± SEM and are representative of at least two independent experiments. *P* value was determined by unpaired two-tailed *t* tests (**F**) or two-sided non-parametric permutation test (**G**). Source data are provided as a Source Data file.

https://doi.org/10.1038/s41467-026-70876-4

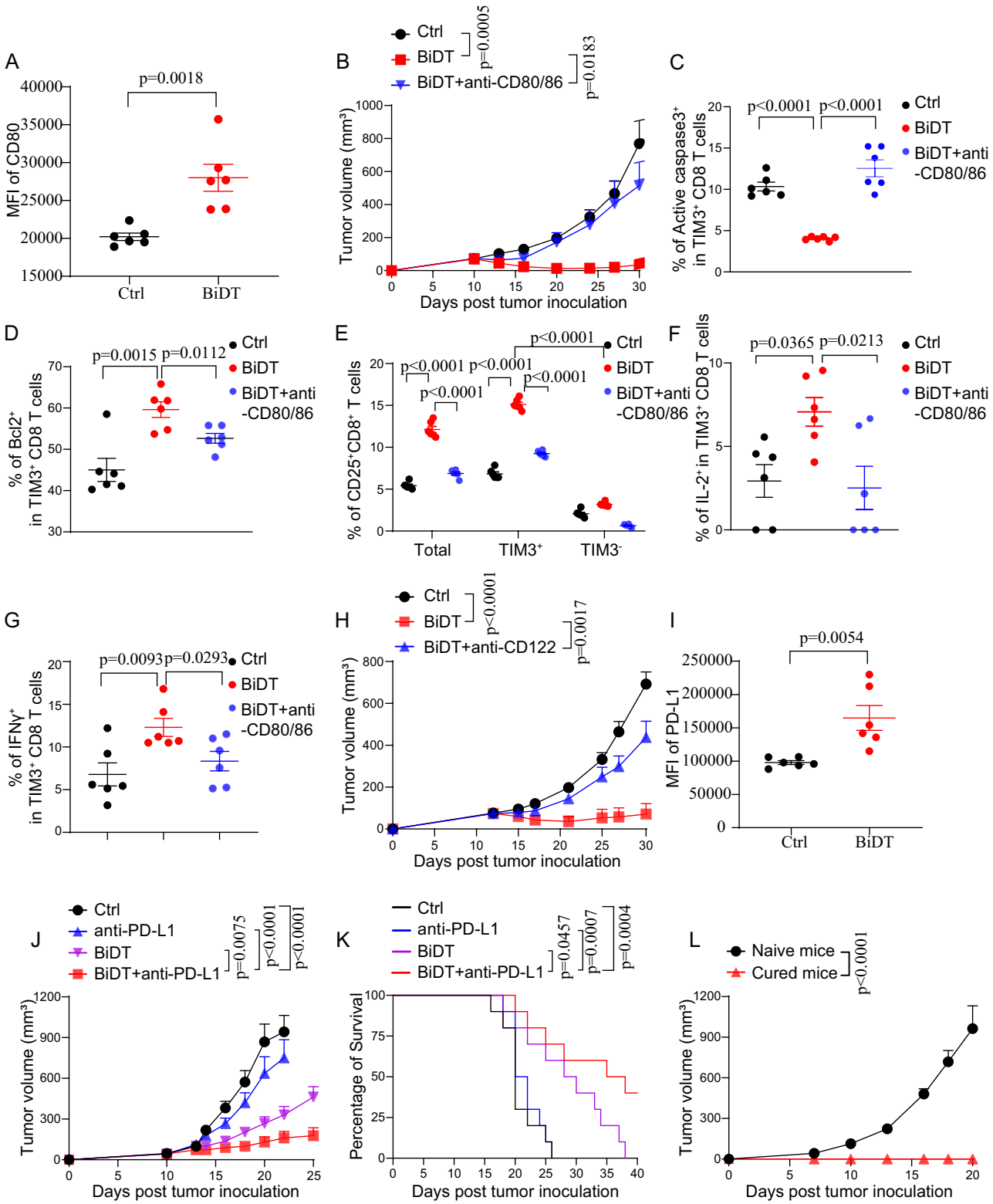

the role of IFN-γ, we administered an IFN-γ neutralizing antibody to BiDT-treated MC38 tumor-bearing mice, which completely abrogated the antitumor effects (Supplementary Fig. 13G). This demonstrates that IFN-γ is essential for BiDT's efficacy. Moreover, administration of anti-CD122 antibodies completely abolished BiDT's antitumor activity (Fig. 6H). This finding underscores the potential importance of DC-mediated T cell activation and IL-2 signaling in antitumor immunity. Thus, it opens avenues for more potent combinational strategies for more advanced cancer.

In summary, BiDT facilitates physical and functional crosstalk between DC and TIM3⁺ exhausted CD8⁺ T cells inside the TME. IFN-I-mediated activation enhances DC's expression of CD80/86, enabling them to deliver co-stimulatory signals to TIM3⁺ exhausted T cells via a physical bridge formed by BiDT. This interaction reactivates exhausted T cells, restores IL-2 signaling, and subsequently amplifies IFN-γ production. Ultimately, this cascade drives robust antitumor immunity.

Fig. 6 | Co-stimulatory signaling and IL-2 signaling are required for BiDT-mediated antitumor effects. A MC38 tumor-bearing female C57BL/6 mice ($n = 6$/group) were treated with 25 μg BiDT on day 16. Tumor tissues were collected 72 h after injection. Expression of CD80 in tumor-infiltrating DCs was measured by FACS. **B** MC38-bearing female C57BL/6 mice ($n = 7$/group) were treated with 25 μg BiDT on days 13, 16 and 19 after tumor inoculation. For blocking CD80/86, anti-CD80 and anti-CD86 were administrated twice a week for 2 weeks. **C**–**G** MC38 tumor-bearing female C57BL/6 mice ($n = 6$/group) were treated with 25 μg BiDT on day 16 after tumor inoculation. For blocking CD80/86, anti-CD80 and anti-CD86 were administrated on day 16 after tumor inoculation. Tumor tissues were collected on day 19 after tumor inoculation. The percentage of active caspase3$^+$ in TIM3$^+$CD8$^+$T cells (**C**), the percentage of Bcl-2$^+$ in TIM3$^+$CD8$^+$T cells (**D**), the percentage of CD25 in total CD8$^+$T cells/TIM3$^+$ CD8$^+$T cells and TIM3$^-$CD8$^+$T cells (**E**), the percentage of IL-2$^+$ in TIM3$^+$CD8$^+$T cells (**F**), the percentage of IFN-γ$^+$ in TIM3$^+$CD8$^+$T cells (**G**) were measured by FACS. **H** MC38-bearing female C57BL/6 mice ($n = 7$/group) were treated with BiDT, or BiDT + anti-CD122 on days 13, 16 and 19 after tumor inoculation. **I** The female C57BL/6 mice ($n = 6$/group) were euthanized, and tumor tissues were collected 72 h after BiDT treatment. Expression of PD-L1 in DC was measured by FACS. **J**, **K** B16F10-bearing female C57BL/6 mice ($n = 10$/group) were i.p. treated with 50 μg BiDT and/or 150 μg anti-PD-L1 on days 9, 12 and 15 after tumor inoculation. Tumor volume (**J**) was measured as indicated, and the mouse survival curve was shown in (**K**). **L** 30 days after treatment with BiDT and anti-PD-L1, cured B16F10-bearing female mice ($n = 5$/group) were re-challenged with 2×10^6 B16F10 cells. Data are shown as mean ± SEM and are representative of at least two independent experiments. *P* value was determined by unpaired two-tailed *t* tests (**A**, **I**, **L**) or One-way ANOVA with Tukey's test (**B**–**G**, **H**, **J**). Survival curve was compared using the log-rank test (**K**). Source data are provided as a Source Data file.

BiDT overcomes immune checkpoint blockade resistance in cold tumors

Resistance to immune checkpoint blockade (ICB) in immunologically "cold" tumors, remains a major clinical challenge[39,40]. The B16F10 melanoma, a classic cold tumor model, exhibits poor responsiveness to ICB[41]. Importantly, similar to the MC38 model, the B16F10 model is established in C57BL/6 mice, and tumor-infiltrating CD8$^+$ T cells in this model also exhibit high TIM3 expression, consistent with the MC38 model (Supplementary Fig. 14A, B). We therefore investigated whether BiDT treatment could effectively eradicate cold tumors.

While BiDT monotherapy extended survival in the B16F10 model, it failed to achieve complete tumor eradication, with all tumors eventually recurring (Supplementary Fig. 14C). Analysis of the underlying mechanism revealed that PD-L1 expression was upregulated in DC within the TME following BiDT treatment (Fig. 6I and Supplementary Fig. 14D). This upregulation can be primarily attributed to the IFN-α component within the BiDT[42,43]. This IFNα-driven PD-L1 upregulation on DC indicated combining PD-L1 blockade with BiDT to counteract this adaptive resistance mechanism.

In the B16F10 model, anti-PD-L1 overcomes BiDT therapy resistance, achieving complete eradication in 40% cases (Fig. 6J, K). Critically, BiDT not only acted synergistically to eliminate tumors but also induced durable immune memory, preventing tumor recurrence upon rechallenge (Fig. 6L). These results position BiDT as a promising solution to the unmet clinical challenge of ICB resistance even in cold tumors, leveraging its dual ability to enhance T cell activation and reprogram immunologically inert tumor microenvironments.

Pro-BiDT maintained maximal antitumor activities with minimal toxicities

Despite FDA approval for melanoma and lymphoma treatment, the clinical use of type I IFN has been limited by severe systemic toxicity[44]. Acute side effects, such as flu-like symptoms, are driven by cytokine release (e.g., TNF, IL-1, IL-6), while subacute and chronic toxicities include hematological disorders such as leukopenia and thrombocytopenia[45]. To address these limitations, we engineered TIM3-ProIFNα (Pro-BiDT) (Fig. 7A), a tumor-activated prodrug derived from BiDT. Pro-BiDT incorporates a ProIFNα whereby the IFNα receptor is conjugated to matrix metalloproteinase (MMP) substrate, preventing IFNα from binding its receptor in peripheral tissues. MMPs, which are highly expressed in various tumor types and contribute to tumor angiogenesis and invasion, can cleave ProIFNα, ensuring activation of IFNα specifically within the TME[46,47].

Pro-BiDT demonstrated potent antitumor activity comparable to BiDT (Fig. 7B). Importantly, Pro-BiDT significantly reduced systemic toxicity. While BiDT caused severe weight loss and elevated levels of pro-inflammatory cytokines (e.g., MCP-1, TNF, IFN-γ, IL-6), Pro-BiDT-treated mice showed no significant weight loss or cytokine elevation (Fig. 7C, D and Supplementary Fig. 15A–C). Additionally, BiDT-induced thrombocytopenia and leukopenia, whereas Pro-BiDT preserved normal platelet and leukocyte counts (Fig. 7E, F). The efficacy of Pro-BiDT was comparable even in the cold tumor model B16F10 (Fig. 7G). In summary, Pro-BiDT maintains robust antitumor efficacy while minimizing systemic toxicity, offering a promising therapeutic strategy to overcome the limitations of conventional IFNα-based therapies.

Discussion

The initiation of T cell priming has been attributed to DC-T cell interactions in DLNs[7]. The importance and molecular mechanism of DC-T cell crosstalk inside the TME for local immunity have not been well defined[13]. It is hard to define whether and how enhanced DC-T cell crosstalk could rescue dysfunctional T cells inside the TME. Here, we demonstrate that restoring functional interactions between intratumoral DC and exhausted T cells via a BiDT not only reactivates T cells but also establishes durable antitumor immunity. Our findings underscore the indispensable role of intratumoral DC in orchestrating T cell reactivation, highlighting that effective DC-T cell interactions within the TME, rather than solely in lymphoid organs, are essential to counteract T cell exhaustion (Fig. 8). This paradigm shift provides a blueprint for next-generation immunotherapies designed to target the TME directly.

Mechanistically, BiDT exerts its therapeutic effects through a dual-targeting mechanism: it binds TIM3 on exhausted CD8$^+$ T cells to block inhibitory signaling, while simultaneously engaging IFNAR on DC to deliver IFNα-driven activation signals. By physically bridging these two cell types, BiDT establishes a functional immune synapse that drives the key process: IFNα-mediated DC activation, which upregulates co-stimulatory ligands (CD80/86) to reactivate exhausted T cells. This signaling axis rescues exhausted T cells from apoptosis and restores the IL-2 signal and IFN-γ-secreting function in exhausted T cells[11].

Crucially, BiDT's effectiveness hinges on pre-existing TILs and DC in the TME. Two key experiments underscore this dependency. First, blocking lymphocyte exit from lymph nodes with FTY720 did not compromise BiDT's antitumor activity, ruling out reliance on peripheral T cell recruitment. Second, transferring tumor fragments into lymphocyte-deficient *Rag1*$^{-/-}$ mice demonstrated that intratumoral TILs alone can drive BiDT-mediated tumor regression. These findings diverge from conventional immunotherapies, such as cancer vaccines that rely on T cell priming by DC in lymphoid organs and highlight the critical antitumor function of intratumoral DC.

A key translational implication of our work is the demonstrated synergy between BiDT and PD-1/PD-L1 blockade in eradicating immunologically cold tumor. IFNα-induced PD-L1 upregulation on DC creates a compensatory immunosuppressive feedback loop[14]. Anti-PD-L1 antibodies could block the PD-L1/PD-1 pathway and break this immunosuppressive feedback loop. Moreover, anti-PD-L1 antibodies disrupted the PD-L1/CD80 cis interaction, enhanced CD80/86-CD28 engagement, and amplified CD28 co-stimulation, creating potential synergies with BiDT[48]. By combining BiDT with PD-L1 blockade, we

https://doi.org/10.1038/s41467-026-70876-4

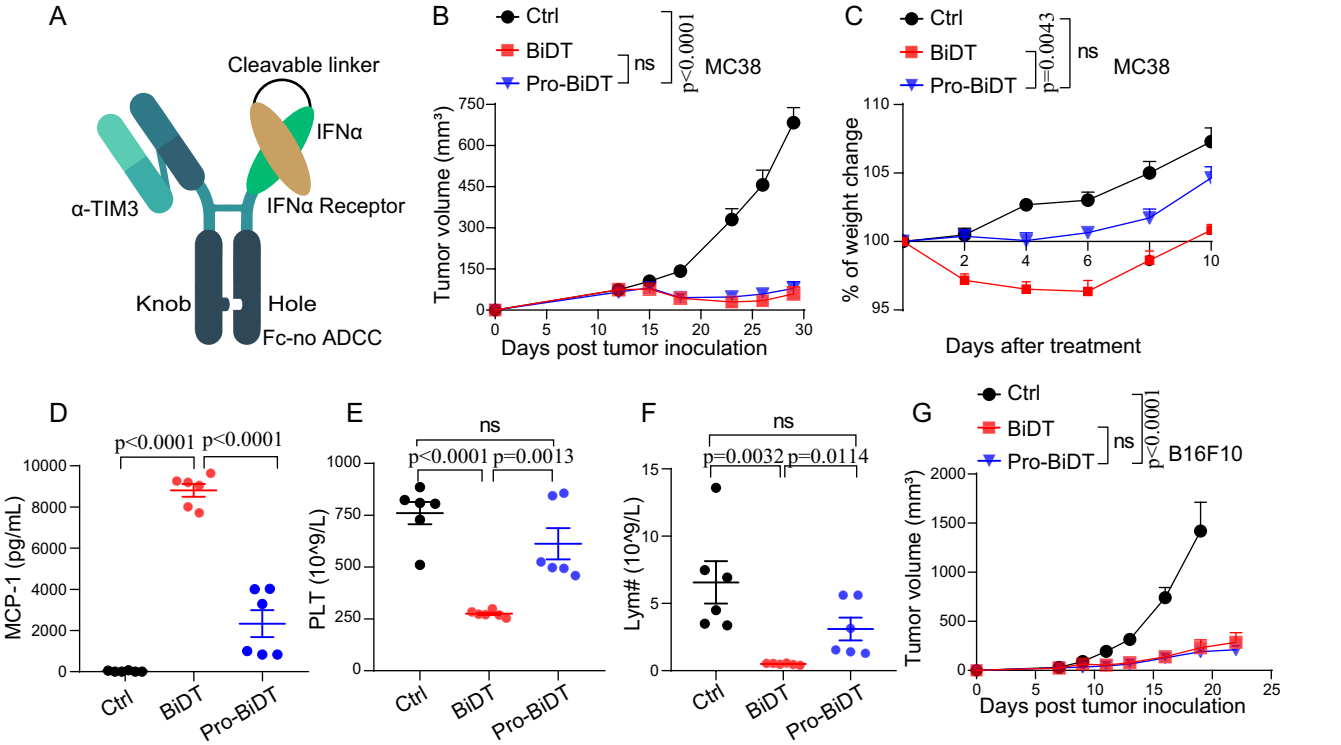

Fig. 7 | Pro-BiDT maintained maximal antitumor activities with minimal toxicities. A Schematic diagram of Pro-BiDT. **B**, **C** MC38-bearing female C57BL/6 mice ($n = 6$/group) were treated i.p. with equal molar amounts (600 pmol) of BiDT or Pro-BiDT on days 13, 16 and 19 post-inoculation. Tumor volumes (**B**) and Body weights (**C**) were measured as indicated. **D**–**F** MC38-bearing female mice ($n = 6$/group) were treated i.p. with equal molar amounts (600 pmol) of BiDT or Pro-BiDT on day 13 after tumor inoculation. Blood samples were collected 24 h after the first injection. Serum MCP-1 levels were measured by cytometric bead assay (**D**). Complete blood count was measured (**E**, **F**). **G** B16F10-bearing female C57BL/6 mice ($n = 6$/group) were i.p. treated with equal molar amounts (600 pmol) of BiDT or Pro-BiDT on days 8, 11 and 14 post-inoculation. Tumor volumes were measured as indicated (**G**). Data are shown as mean ± SEM and are representative of at least two independent experiments. *P* value was determined by One-way ANOVA with Tukey's test (**B**–**G**). Source data are provided as a Source Data file.

achieved complete tumor eradication in treated mice bearing an advanced tumor, a striking improvement over either therapy alone. Our results position BiDT as a rational partner for ICB in tumors with low T cell infiltration-a common clinical challenge in immunologically "cold" tumors.

The clinical application of IFNα has been limited by severe systemic toxicity, including acute flu-like symptoms and hematological disorders. To address this, we engineered Pro-BiDT, a tumor-activated prodrug that incorporates an IFNα receptor linked by an MMP-cleavable spacer. Pro-IFNα is selectively activated by tumor-associated MMPs, minimizing systemic toxicity while extending the half-life of IFNα[49]. By leveraging TIM3's prevalent expression on TILs, Pro-BiDT achieves targeted delivery to the TME, further enhancing its therapeutic index.

In conclusion, we designed BiDT, a bispecific engager targeting TIM3 on exhausted T cells and IFNAR on DC, to enhance the intratumoral DC-T cell interactions and reactivate exhausted T cell function. This dual action revived T cell activity through IL-2/STAT5 signaling and apoptosis reversal, relying solely on cross-presentation between pre-existing intratumoral TILs and DC. By engineering Pro-BiDT, a tumor-activated prodrug, we minimized systemic toxicity while retaining efficacy. This strategy overcomes ICB resistance in cold tumors. These findings provide a foundation for future studies aimed at improving immunotherapeutic strategies and patient outcomes.

Methods

Mice

C57BL/6 and *Rag1*$^{-/-}$ mice were obtained from GemPharmatech Co., Ltd (Stock Number: N000013 and T004753, respectively). *Lyz2*-Cre and *Havcr2*$^{fl/fl}$ mice were provided by Gencheng Han (Beijing Institute of Basic Medical Sciences, Beijing). *Cd4*-Cre mice were a gift from Xiaohuan Guo (Tsinghua University, Beijing). *Ifnar1*$^{-/-}$ and *Ifnar1*$^{fl/fl}$ mice were sourced from Hua Peng (Institute of Biophysics, Chinese Academy of Sciences, China). *Zbtb46*-Cre mice were provided by Li Wu (Tsinghua University, Beijing). Female mice (7–8 weeks old) were selected based on their lower aggression, which facilitates group housing and reduces management requirements. All mice were maintained under specific pathogen-free conditions with 10/14 dark/light cycle, 20–26 °C, and 30–70% humidity. Mice were euthanized by CO_2 asphyxiation followed by cervical dislocation. Experimental animals and control animals were bred separately. All studies were approved by the Animal Care and Use Committee of Tsinghua University. The maximum tumor size allowed by the Animal Care and Use Committee of Tsinghua University is 1500 mm^3, and we have adhered to this size limitation in our experiments.

Cell lines and reagents

MC38 cell line was purchased from Cytion (#305223). B16F10 cell line was obtained from the American Type Culture Collection (#CR6475). MC38-OVA was generated by selecting single-cell clones following lentiviral transfection with an OVA-expressing construct. *Ifnar1*$^{-/-}$ MC38 cell line was sourced from Mingzhao Zhu (Institute of Microbiology, Chinese Academy of Sciences, China). MC38, B16F10, and B16F10-OVA cells were cultured in Dulbecco's Modified Eagle's Medium (DMEM) supplemented with 10% heat-inactivated fetal bovine serum, penicillin (100 U/ml), and streptomycin (100 μg/ml) at 37 °C under 5% CO_2. Antibodies used in this study included anti-CD4 (GK1.5, Bioxcell #BE0003-1), anti-CD8 (53-5.8, Bioxcell #BE0004-1), anti-NK1.1

https://doi.org/10.1038/s41467-026-70876-4

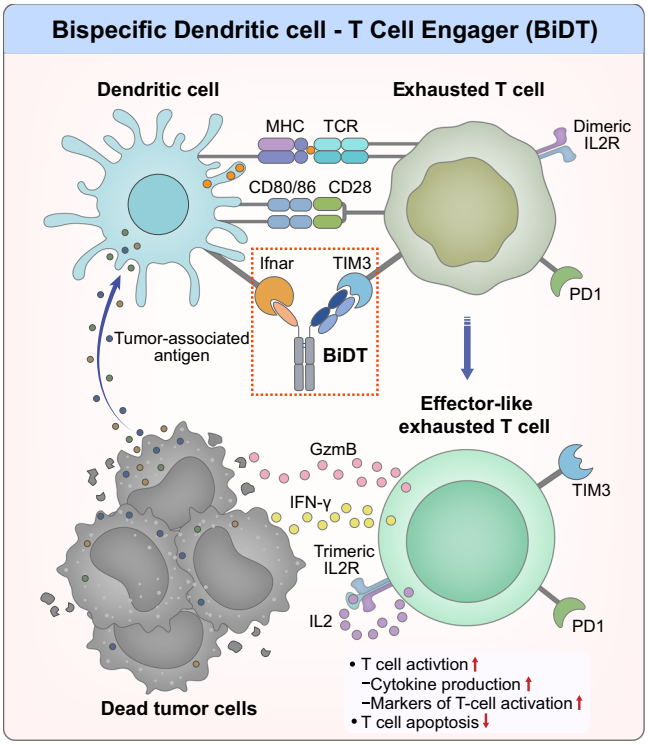

Fig. 8 | Schematic of hypothesized working model. Most tumor-specific $CD8^+$ T cells in the TME are exhausted with upregulation of several co-inhibitory molecules, such as TIM3, contributing to the ineffectiveness of immunotherapies. There is a critical need to reactivate these exhausted T cells. We developed a bispecific dendritic cell-T cell engager (BiDT)-the anti-TIM3-IFNα fusion protein (TIM3-IFNα). This reagent simultaneously targets the TIM3 on exhausted TILs, binding to IFNAR on DCs, which activates DCs via IFNα and promotes robust DC/T cell crosstalk within the TME. BiDT reactivated $TIM3^+$ TILs, especially the $TIM3^+$ tumor-specific, ultimately enhancing their antitumor activity. Mechanically, BiDT allows DC to reactivate T cells by enhancing the IL-2 signal pathway of TILs through not only first signal but also CD80/86-CD28 co-stimulation, leading to reactivating TILs to subsequently increase production of other cytokines, especially IFN-γ. Furthermore, dead tumor cells killed by TILs in the TME also provide tumor-associated antigen for DCs. Type I IFN educated those DCs to further enhance the antigen presentation.

(PK136, Bioxcell #BE0036), anti-CSF1R (AFS98, Bioxcell #BE0213), anti-IFN-γ (XMG1.2, Bioxcell #BE0050), anti-CD80 (16-10A1, Bioxcell, #BE0024), anti-CD86 (GL-1, Bioxcell, #BE0025), and anti-IL-2Rβ (TM-β1, Bioxcell, #BE0298), all purchased from Bio X Cell. FTY720 was obtained from Sigma-Aldrich. A full list of the antibodies used in this study is provided in Supplementary Table 1.

Tumor inoculation and treatment

MC38 cells (5×10^5), MC38-OVA cells (1×10^6), *Ifnar1*$^{-/-}$ MC38 cells (1×10^6), or B16F10 cells (3×10^5) were subcutaneously injected into the right flank of mice. Tumor volume was measured twice weekly and calculated using the formula: length × width × height/2. The criteria for early termination are 1500 mm^3 in tumor volume according to protocol of the Animal Care and Use Committee of Tsinghua University. For specific depletion of Macrophages, NK cells, $CD4^+$ or $CD8^+$ T cells, 500 μg anti-CSF1R, 200 μg anti-NK1.1, 200 μg anti-CD4, or 200 μg anti-CD8 was administered one day before treatment initiation and then twice weekly for two weeks. For anti-CD80 and anti-CD86 treatment, 200 μg anti-CD80 and CD86 were administered on the day of treatment initiation and then twice weekly for two weeks. For IL-2 or IFN-γ neutralization, 500 μg anti-IFN-γ was administered on the day of treatment initiation and then twice weekly for two weeks. To inhibit lymphocyte trafficking, FTY720 was administered at 20 μg one day prior to treatment initiation, then every other day for two weeks.

Production of BiDT and Pro-BiDT fusion protein

On the basis of the heterodimeric Fc variant KiHss-AkKh technology[50], the Fab fragment of anti-TIM3 was fused with the knob variant Fc region, and the IFNα or ProIFNα was fused with the hole variant Fc region. During the ProIFNα protein, the IFNα receptor and IFNα were joined with an MMP linker, which can be cleaved by MMP14. The entire sequence was then cloned into the pEE12.4 vector (Lonza). The anti-TIM3-knobs and IFNα-hole plasmids or ProIFNα-hole plasmids were transiently transfected into 293F cells at a ratio of 1:1. BiDT and Pro-BiDT were generated by transient co-transfection of two arms of plasmids into FreeStyle 293F cells. Supernatants were collected on day 7 after transfection. The supernatant containing bispecific antibodies was purified using Protein A affinity chromatography according to the manufacturer's protocol.

Fluorescence imaging

TIM3-IFNα was labeled with Sulfo-Cy5 NHS ester (RuixiBiotech Co., Ltd) and purified to remove unbound Cy5. Cy5-labeled TIM3-IFNα or EGFR-IFNα was intravenously injected into MC38-bearing C57BL/6 mice. Tumor accumulation of the Cy5-labeled proteins was quantified using the IVIS Spectrum imaging system (PerkinElmer). Fluorescence imaging data were analyzed using Living Image software (PerkinElmer).

Flow cytometry

Mice were intraperitoneally (i.p.) injected with 250 μg of brefeldin A solution (BFA) six hours before being euthanizing. Tumor tissues were harvested, minced into small fragments, and enzymatically digested using 100 μg/ml DNase I (Roche) and 1 mg/ml collagenase IV (Roche) at 37 °C for 40 min. The digested tissues were then filtered through a 70 μm cell strainer to generate single-cell suspensions. Cells were blocked with anti-CD16/32 antibody (clone 93) for 30 min and subsequently stained with fluorochrome-conjugated antibodies for 30 min at 4 °C. For intracellular staining, cells were fixed, permeabilized, and incubated with specific antibodies for 1 h on ice. All fluorescently labeled monoclonal antibodies were obtained from BioLegend or eBioscience. Samples were analyzed using a FACS Calibur or Fortessa flow cytometer, and data were processed using FlowJo software (TreeStar).

TCGA database analysis

Correlation of CD25 expression with DC infiltration or CD86 expression, and correlation of IFN-γ expression with CD25 expression were analyzed using Tumor Immune Estimation Resource (TIMER; https://cistrome.shinyapps.io/timer/).

Sample preparation for scRNA-seq

Live $CD45^+$ cells were sorted from MC38 tumors by FACS, and five biological replicates were amalgamated for library construction. Single-cell transcriptomic libraries were generated using the commercial workflow specified by 10x Genomics. Sequencing was executed on an Illumina NovaSeq 6000 platform (Singleron Biotechnologies, Beijing, China) employing paired-end sequencing with 150 bp read length.

Data analysis for scRNA-seq

Raw sequencing data were processed using Cell Ranger (v7.1.0), and downstream analysis was conducted via R (v4.2.2) and Seurat (v4.1.0). Cells with mitochondrial gene content below 10%, *Hsp* gene content below 3%, n_Feature RNA between 300 and 6000, n_Count RNA below 40000 were retained. Data normalization, scaling and identification of

variable genes were performed via NormalizeData, ScaleData, and FindVariableFeatures, respectively. For dimensionality reduction, 2000 highly variable genes were selected for PCA reduction using RunPCA, followed by 2D visualization using FindNeighbors, FindClusters and RunTSNE or RunUMAP. $CD8^+$ T cells were selected for further clustering and downstream phenotype analysis. Signature gene sets for GSEA analysis were downloaded from mouse MSigDB (the Molecular Signatures Database)[51].

Statistical analysis

Data are presented as mean ± SEM. Statistical analyses were conducted using GraphPad Prism software. *P* values were calculated using unpaired two-tailed Student's *t* tests, paired *t* tests or One-way ANOVA with Tukey's test. Survival curves were compared using the log-rank test. Significance levels are denoted as follows: $^*P < 0.05$, $^{**}P < 0.01$, $^{***}P < 0.001$, and $^{****}P < 0.0001$.

Reporting summary

Further information on research design is available in the Nature Portfolio Reporting Summary linked to this article.

Data availability

All data are included in the Supplementary Information or available from the authors, as are unique reagents used in this Article. The raw numbers for charts and graphs are available in the Source Data file whenever possible. The single-cell RNA-seq data have been deposited in Gene Expression Omnibus under the accession number GSE320312. Correspondence and requests for materials should be addressed to Yang-Xin Fu (yangxinfu@tsinghua.edu.cn), Wenyan Wang (wywang2022@tsinghua.edu.cn) or Xuhao Zhang (xuhaozhang@cqmu.edu.cn). Source data are provided with this paper.

References

1. Clynes, R. A. & Desjarlais, J. R. Redirected T cell cytotoxicity in cancer therapy. *Annu. Rev. Med* **70**, 437–450 (2019).
2. Thommen, D. S. & Schumacher, T. N. T cell dysfunction in cancer. *Cancer Cell* **33**, 547–562 (2018).
3. Chen, L. & Flies, D. B. Molecular mechanisms of T cell co-stimulation and co-inhibition. *Nat. Rev. Immunol.* **13**, 227–242 (2013).
4. Blank, C. U. et al. Defining 'T cell exhaustion. *Nat. Rev. Immunol.* **19**, 665–674 (2019).
5. Das, M., Zhu, C. & Kuchroo, V. K. Tim-3 and its role in regulating anti-tumor immunity. *Immunol. Rev.* **276**, 97–111 (2017).
6. Sakuishi, K. et al. Targeting Tim-3 and PD-1 pathways to reverse T cell exhaustion and restore anti-tumor immunity. *J. Exp. Med.* **207**, 2187–2194 (2010).
7. Eisenbarth, S. C. Dendritic cell subsets in T cell programming: location dictates function. *Nat. Rev. Immunol.* **19**, 89–103 (2019).
8. Esensten, J. H., Helou, Y. A., Chopra, G., Weiss, A. & Bluestone, J. A. CD28 costimulation: from mechanism to therapy. *Immunity* **44**, 973–988 (2016).
9. Acuto, O. & Michel, F. CD28-mediated co-stimulation: a quantitative support for TCR signalling. *Nat. Rev. Immunol.* **3**, 939–951 (2003).
10. Tacke, M., Hanke, G., Hanke, T. & Hunig, T. CD28-mediated induction of proliferation in resting T cells in vitro and in vivo without engagement of the T cell receptor: evidence for functionally distinct forms of CD28. *Eur. J. Immunol.* **27**, 239–247 (1997).
11. Boise, L. H. et al. CD28 costimulation can promote T cell survival by enhancing the expression of Bcl-XL. *Immunity* **3**, 87–98 (1995).
12. Wculek, S. K. et al. Dendritic cells in cancer immunology and immunotherapy. *Nat. Rev. Immunol.* **20**, 7–24 (2020).
13. Marciscano, A. E. & Anandasabapathy, N. The role of dendritic cells in cancer and anti-tumor immunity. *Semin. Immunol.* **52**, 101481 (2021).
14. Liang, Y. et al. Targeting IFNalpha to tumor by anti-PD-L1 creates feedforward antitumor responses to overcome checkpoint blockade resistance. *Nat. Commun.* **9**, 4586 (2018).
15. Diamond, M. S. et al. Type I interferon is selectively required by dendritic cells for immune rejection of tumors. *J. Exp. Med* **208**, 1989–2003 (2011).
16. Deng, L. et al. STING-dependent cytosolic DNA sensing promotes radiation-induced type I interferon-dependent antitumor immunity in immunogenic tumors. *Immunity* **41**, 843–852 (2014).
17. Woo, S. R. et al. STING-dependent cytosolic DNA sensing mediates innate immune recognition of immunogenic tumors. *Immunity* **41**, 830–842 (2014).
18. Sleijfer, S., Bannink, M., Van Gool, A. R., Kruit, W. H. & Stoter, G. Side effects of interferon-alpha therapy. *Pharm. World Sci.* **27**, 423–431 (2005).
19. Ren, Z. et al. Selective delivery of low-affinity IL-2 to PD-1+ T cells rejuvenates antitumor immunity with reduced toxicity. *J. Clin. Invest.* **132**, https://doi.org/10.1172/JCI153604 (2022).
20. Corbett, T. H., Griswold, D. P. Jr., Roberts, B. J., Peckham, J. C. & Schabel, F. M. Jr Tumor induction relationships in development of transplantable cancers of the colon in mice for chemotherapy assays, with a note on carcinogen structure. *Cancer Res.* **35**, 2434–2439 (1975).
21. Lee, H. O. et al. Lineage-dependent gene expression programs influence the immune landscape of colorectal cancer. *Nat. Genet.* **52**, 594–603 (2020).
22. Gide, T. N. et al. Distinct immune cell populations define response to anti-PD-1 monotherapy and anti-PD-1/Anti-CTLA-4 combined therapy. *Cancer Cell* **35**, 238–255 e236 (2019).
23. Yu, R., Zhu, B. & Chen, D. Type I interferon-mediated tumor immunity and its role in immunotherapy. *Cell Mol. Life Sci.* **79**, 191 (2022).
24. Zhang, X. et al. TIM3-blockade synergizes with IL2 in alleviating intra-tumoral CD8(+)T cell exhaustion. *Nat. Commun.* **16**, 5130 (2025).
25. Dixon, K. O. et al. TIM-3 restrains anti-tumour immunity by regulating inflammasome activation. *Nature* **595**, 101–106 (2021).
26. Ando, M., Ito, M., Srirat, T., Kondo, T. & Yoshimura, A. Memory T cell, exhaustion, and tumor immunity. *Immunol. Med.* **43**, 1–9 (2020).
27. Ganesh, K. & Massague, J. Targeting metastatic cancer. *Nat. Med.* **27**, 34–44 (2021).
28. Yang, X. et al. Targeting the tumor microenvironment with interferon-beta bridges innate and adaptive immune responses. *Cancer Cell* **25**, 37–48 (2014).
29. Khalaf, S. et al. Differential expression of TIM-3 in circulation and tumor microenvironment of colorectal cancer patients. *Clin. Immunol.* **215**, https://doi.org/10.1016/j.clim.2020.108429 (2020).
30. Mombaerts, P. et al. RAG-1-deficient mice have no mature B and T lymphocytes. *Cell* **68**, 869–877 (1992).
31. Liu, L. et al. Rejuvenation of tumour-specific T cells through bispecific antibodies targeting PD-L1 on dendritic cells. *Nat. Biomed. Eng.* **5**, 1261–1273 (2021).
32. Xue, D. et al. A tumor-specific pro-IL-12 activates preexisting cytotoxic T cells to control established tumors. *Sci. Immunol.* **7**, https://doi.org/10.1126/sciimmunol.abi6899 (2022).
33. Liang, Y., Hannan, R. & Fu, Y.-X. Type I IFN activating type I dendritic cells for antitumor immunity. *Clin. Cancer Res.* **27**, 3818–3824 (2021).
34. Wolf, Y., Anderson, A. C. & Kuchroo, V. K. TIM3 comes of age as an inhibitory receptor. *Nat. Rev. Immunol.* **20**, 173–185 (2020).
35. Wu, W. et al. IL-2Rα-biased agonist enhances antitumor immunity by invigorating tumor-infiltrating CD25+CD8+ T cells. *Nat. Cancer* **4**, 1309–1325 (2023).
36. Spolski, R., Li, P. & Leonard, W. J. Biology and regulation of IL-2: from molecular mechanisms to human therapy. *Nat. Rev. Immunol.* **18**, 648–659 (2018).

37. Boyman, O. & Sprent, J. The role of interleukin-2 during homeostasis and activation of the immune system. *Nat. Rev. Immunol.* **12**, 180–190 (2012).
38. Bae, J. et al. IL-2 delivery by engineered mesenchymal stem cells re-invigorates CD8(+) T cells to overcome immunotherapy resistance in cancer. *Nat. Cell Biol.* **24**, 1754–1765 (2022).
39. Zhang, J., Huang, D., Saw, P. E. & Song, E. Turning cold tumors hot: from molecular mechanisms to clinical applications. *Trends Immunol.* **43**, 523–545 (2022).
40. Lin, K. X. et al. PD-1 and PD-L1 inhibitors in cold colorectal cancer: challenges and strategies. *Cancer Immunol. Immunother.* **72**, 3875–3893 (2023).
41. Zhang, T. et al. Up-regulated PLA2G10 in cancer impairs T cell infiltration to dampen immunity. *Sci. Immunol.* **9**, eadh2334 (2024).
42. Muhlbauer, M. et al. PD-L1 is induced in hepatocytes by viral infection and by interferon-alpha and -gamma and mediates T cell apoptosis. *J. Hepatol.* **45**, 520–528 (2006).
43. Bald, T. et al. Immune cell-poor melanomas benefit from PD-1 blockade after targeted type I IFN activation. *Cancer Discov.* **4**, 674–687 (2014).
44. Yu, R., Zhu, B. & Chen, D. Type I interferon-mediated tumor immunity and its role in immunotherapy. *Cell. Mol. Life Sci.* **79**, https://doi.org/10.1007/s00018-022-04219-z (2022).
45. Kirkwood, J. M. et al. Mechanisms and management of toxicities associated with high-dose interferon alfa-2b therapy. *J. Clin. Oncol.* **20**, 3703–3718 (2002).
46. Deryugina, E. I. & Quigley, J. P. Matrix metalloproteinases and tumor metastasis. *Cancer Metastasis Rev.* **25**, 9–34 (2006).
47. Gobin, E. et al. A pan-cancer perspective of matrix metalloproteases (MMP) gene expression profile and their diagnostic/prognostic potential. *BMC Cancer* **19**, 581 (2019).
48. Mayoux, M. et al. Dendritic cells dictate responses to PD-L1 blockade cancer immunotherapy. *Sci. Transl. Med.* **12**, https://doi.org/10.1126/scitranslmed.aav7431 (2020).
49. Cao, X. et al. Next generation of tumor-activating type I IFN enhances anti-tumor immune responses to overcome therapy resistance. *Nat. Commun.* **12**, 5866 (2021).
50. Ridgway, J. B., Presta, L. G. & Carter, P. Knobs-into-holes' engineering of antibody CH3 domains for heavy chain heterodimerization. *Protein Eng.* **9**, 617–621 (1996).
51. Subramanian, A. et al. Gene set enrichment analysis: a knowledge-based approach for interpreting genome-wide expression profiles. *Proc. Natl. Acad. Sci. USA* **102**, 15545–15550 (2005).

Acknowledgements

We are grateful to Hua Peng (Institute of Biophysics, Chinese Academy of Sciences, Beijing) for *Ifnar1*$^{-/-}$ and *Ifnar1*$^{fl/fl}$ mice. Li Wu (Tsinghua University, Beijing) for *Zbtb46*-Cre mice; Gencheng Han (Beijing Institute of Basic Medical Sciences, Beijing) for *Lyz2*-Cre and *Havcr2* $^{fl/fl}$ mice; Xiaohuan Guo (Tsinghua University, Beijing) for *Cd4*-Cre mice. We thank Mingwan Tang, Yutong Fu, Weian Cao, and Li Yu for providing experiment materials and helpful discussions. We thank the faculty in the animal facility of Tsinghua University. This work was supported by grants from the National Natural Science Foundation of China (82250710684, to Y-X.F., 32370967 to W.W., 32300773 to X.S.) and International Postdoctoral Exchange Fellowship Program (to X. Zhang).

Author contributions

Conceptualization: X.Z., Y.G., W.H. and Y-X. F Methodology: X.Z., Y.G., W.H., Y.L., X.Y., X.S., H.L., H.L., X.Y., Y.G. Investigation: X.Z., Y.G., W.H., W.W., M.Z., H.P. Funding acquisition: X.Z., W.W., and Y-X.F. Supervision: W.W., Y-X. F. Writing – original draft: X.Z., Y.G., W.H. Writing – review & editing: X.Z., Y.G., W.H. W.W. and Y-X.F.

Competing interests

The authors declare no competing interests.

Additional information

Supplementary information The online version contains supplementary material available at https://doi.org/10.1038/s41467-026-70876-4.

Correspondence and requests for materials should be addressed to Xuhao Zhang, Wenyan Wang or Yang-Xin Fu.

Peer review information *Nature Communications* thanks Dirk Schadendorf and the other, anonymous, reviewer(s) for their contribution to the peer review of this work. A peer review file is available.